Supporting Information for

Conversion of Electrochemically Deposited Aragonite Crystallites to Perovskite through Ion Exchange

William D. Leal[†], Caroline L. Bergeron[†], Tyler J. Rutherford[†], Marek B. Majewski[†]*

[†]*Department of Chemistry and Biochemistry and Centre for NanoScience Research, Concordia University, Montreal, QC, Canada, H4B 1R6.*

Email: marek.majewski@concordia.ca

Experimental Procedures

1. General Methods

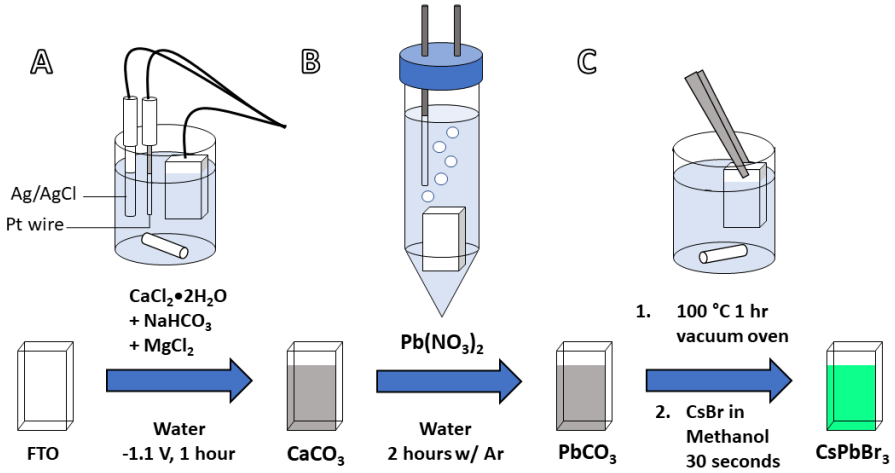

Figure S1. Reaction scheme for the electrochemical deposition of $CaCO_3$ and subsequent conversion to perovskite $CsPbBr_3$ via ion exchange reactions. (A) Experimental setup for electrochemical deposition of $CaCO_3$ on FTO. (B) $CaCO_3$ microstructures are left in an airtight vessel, a centrifuge tube with two holes pierced through its cap, while Ar gas is sparged through the reaction solution. (C) After being dried in a vacuum oven for 1 hour, the sample is held by forceps in the reaction mixture for 30 seconds.

Results and Discussion

1. Structural Analysis

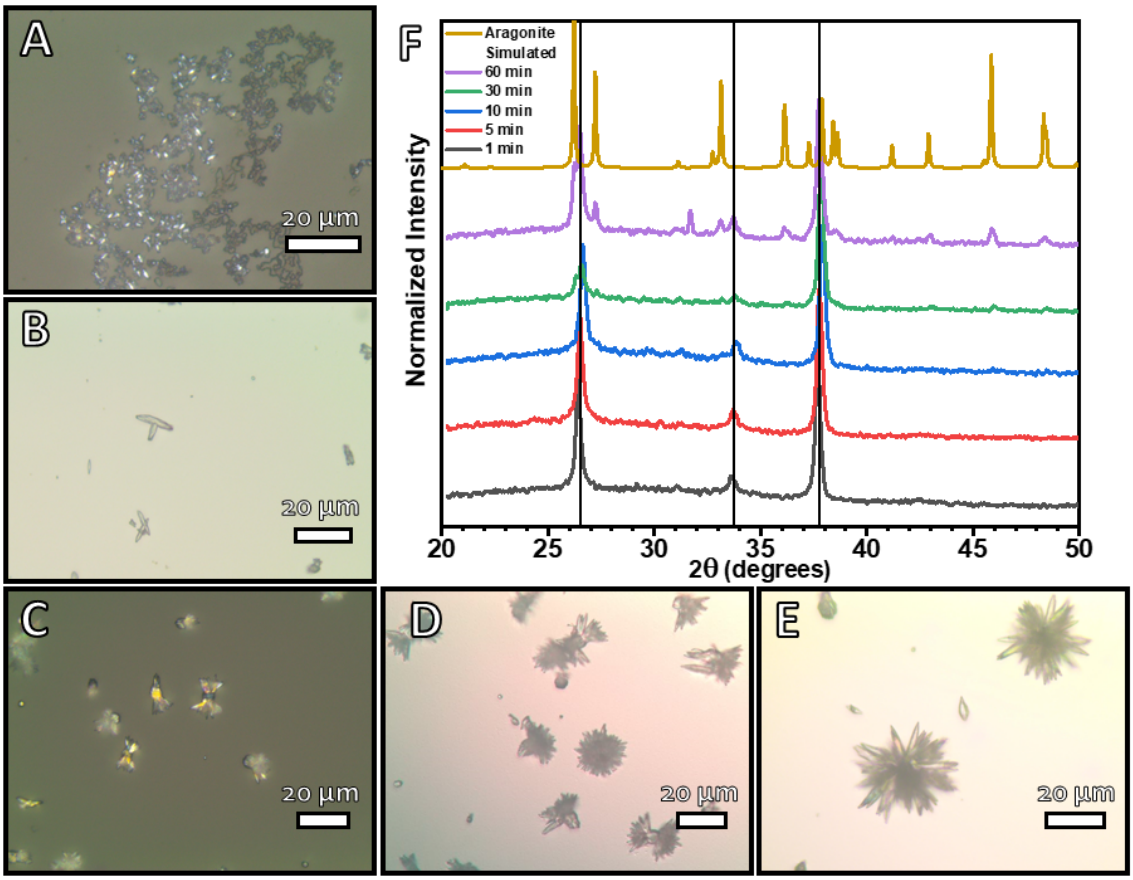

Figure S2. Optical microscope images taken at 40× magnification of $CaCO_3$ crystallites electrochemically deposited for (A) 1, (B) 5, (C) 10, (D) 30, and (E) 60 minutes on FTO with (F) their respective powder X-ray diffraction (PXRD) patterns compared to the simulated pattern for aragonite $CaCO_3$ (ICSD 157993). The reflections outlined by vertical black lines are due to the FTO substrate.

2. Elemental Composition Analysis

$CaCO_3$			$PbCO_3$			$CsPbBr_3$		
Element	**Atomic %**	**Expected Atomic %**	**Element**	**Atomic %**	**Expected Atomic %**	**Element**	**Atomic %**	**Expected Atomic %**
C	**20.1**	**20**	**C**	**34.7**	**20**	**C**	**25.5**	**0**
O	**60.9**	**60**	**O**	**51.9**	**60**	**O**	**52.9**	**0**
Ca	**17.5**	**20**	**Ca**	**0**	**0**	**Ca**	**3.0**	**0**
Pb	**0**	**0**	**Pb**	**13.3**	**20**	**Pb**	**10.5**	**20**
Cs	**0**	**0**	**Cs**	**0**	**0**	**Cs**	**3.8**	**20**
Br	**0**	**0**	**Br**	**0**	**0**	**Br**	**4.1**	**60**

Table S1. SEM-EDS elemental composition analysis of microstructures after electrochemical deposition of $CaCO_3$ and conversion to $PbCO_3$ and $CsPbBr_3$.

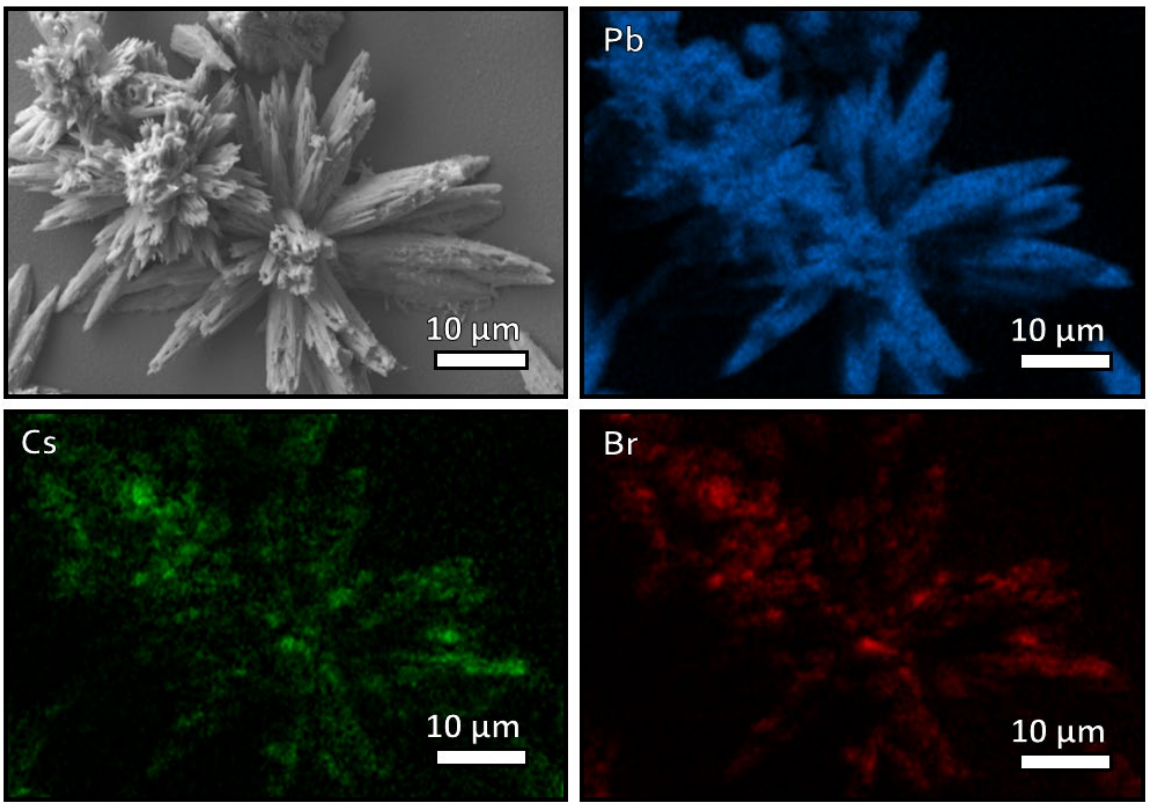

Figure S3. SEM micrograph of microstructure after lead nitrate and cesium bromide conversion steps (top left) with EDS map analyses of Pb, Cs, and Br. Mapping analysis of Pb in Figure S3 shows a clear picture of Pb residing in the microstructure. Analyses of Cs and Br show similar results, but to a less intense degree. Though it is a fainter signal compared to that of Pb, Cs and Br can be seen in the microstructure as well.

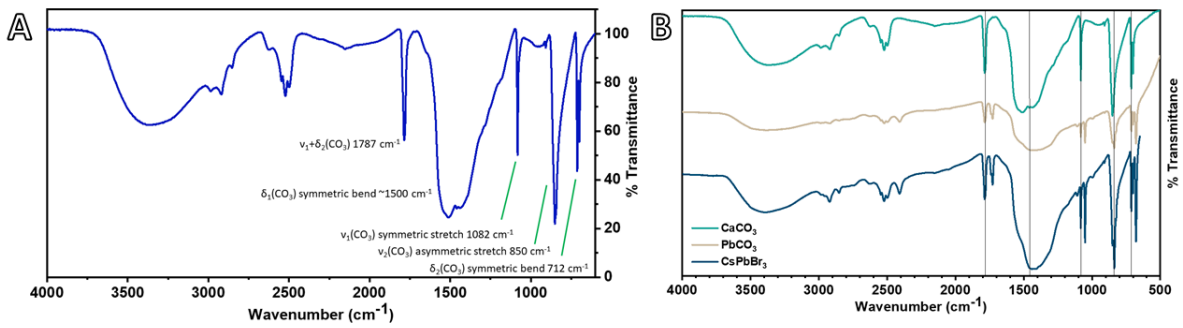

Figure S4. Diffuse reflectance infrared Fourier transform spectroscopic data for (A) electrochemically deposited $CaCO_3$ microstructures with peak assignments and (B) as-deposited $CaCO_3$ compared to microstructures converted to $PbCO_3$ and $CsPbBr_3$. The subsequent traces in Figure S4B, taken after conversion to $PbCO_3$ and $CsPbBr_3$, contain the same peaks as seen in the spectrum of $CaCO_3$, but also show a secondary set of peaks slightly red shifted in energy. This occurs because of the formation of a core/shell structure where the electrochemically deposited $CaCO_3$ microstructures are converted to $PbCO_3$ up to a certain depth but not completely. As such, both $CaCO_3$ and $PbCO_3$ exist in the sample after exposure to the concentrated $Pb(NO_3)_2$ aqueous solution, and this is reflected in the results shown in Figure S4. The $CsPbBr_3$ trace looks identical to that of $PbCO_3$ as the amount of $PbCO_3$ that has been converted to $CsPbBr_3$ is likely too small to have caused any changes in the IR spectrum of the final material. This demonstrates the lack of surface sensitivity of DRIFTS and the need for more sensitive methods of characterization.

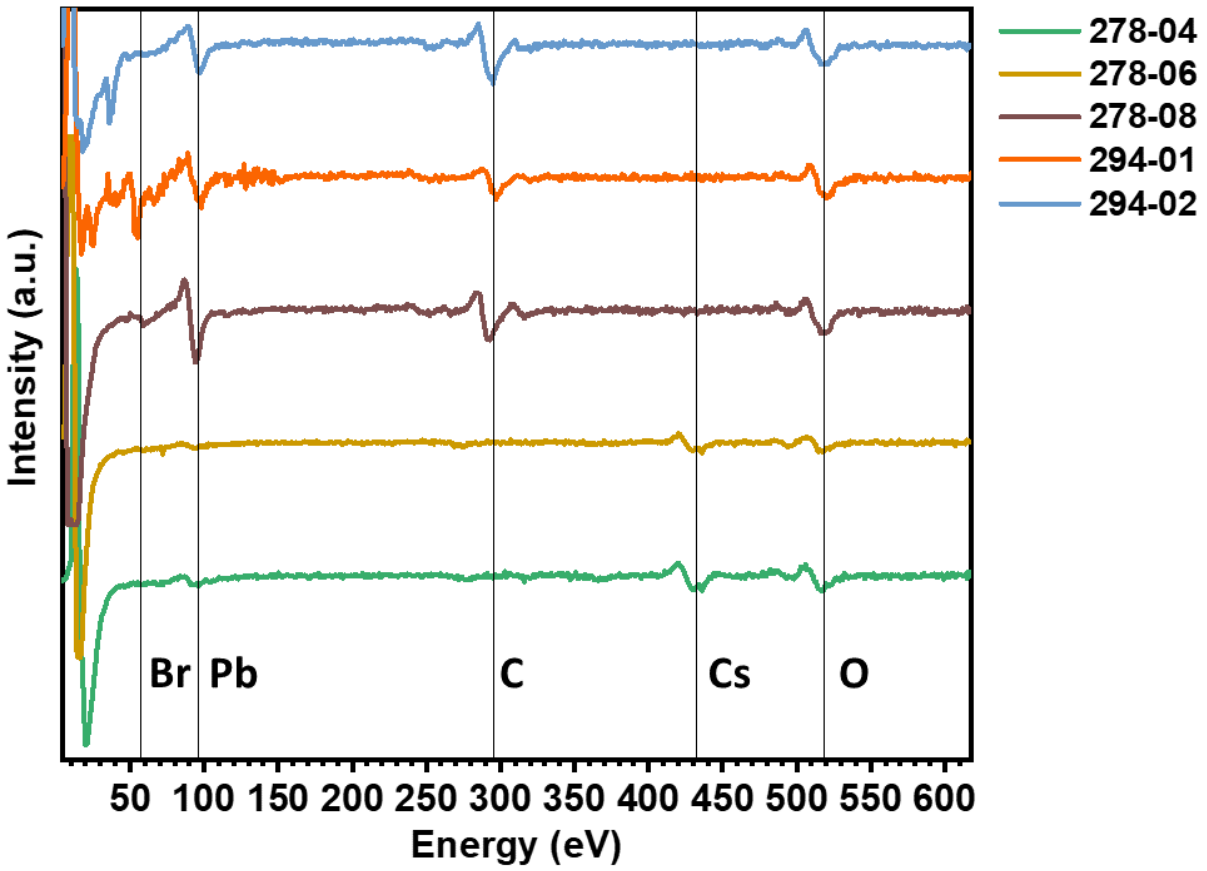

Figure S5. Auger Electron Spectroscopic (AES) data taken from various points on two different samples with characteristic energies outlined and labelled for Br, Pb, C, Cs, and O. Samples are numbered 278 and 294 and were analyzed at different positions on the samples. These different analyses are denoted as run numbers after the sample number in the legend of Figure S5.

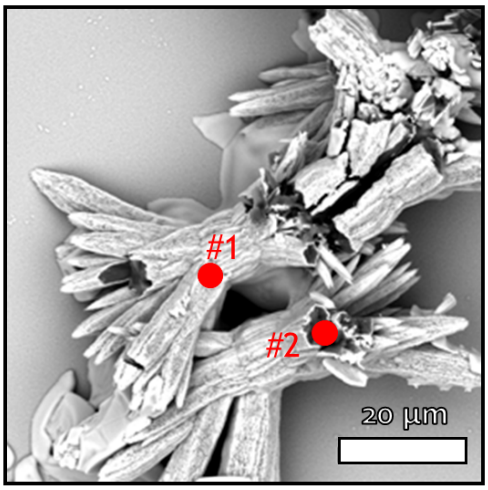

Spot#1

Element	Atomic%	Expected Atomic%
O	50.14	0
C	22.61	0
Pb	18.87	20
Ca	7.01	0
Cs	0.71	20
Br	0.67	60

Spot#2

Element	Atomic%	Expected Atomic%
O	56.08	60
C	22.61	20
Pb	20.53	20
Ca	0.33	0
Cs	0.25	0
Br	0.20	0

Figure S6. Backscattered electron scanning mode SEM micrograph of fractured microstructure resulting from full conversion process with accompanying SEM-EDS analysis of surface and exposed interior.

Sample ID	[Ca](ppm)	[Br](ppm)	[Cs](ppm)	[Pb](ppm)	Br:Cs by element mass
299	4.20E-01	4.38E-02	2.54E-02	1.20E+00	2.87
306	4.26E-01	3.21E-02	8.55E-03	1.20E+00	6.24
302	1.17E-01	3.32E-02	1.91E-02	3.76E-01	2.89
309	1.38E-01	3.22E-02	9.18E-03	7.61E-01	5.83
Stock 1	8.41E-03	8.78E-03	0.00E+00	1.31E-02	
Stock 2	6.43E-03	4.81E-03	0.00E+00	0.00E+00	
Stock 3	1.74E-02	2.90E-03	0.00E+00	3.44E-03	

Table S2. Chemical composition of perovskite microstructure samples as determined by inductively coupled plasma – mass spectrometry (ICP-MS) compared to elemental concentrations present in stock digestion solution. The data reported in Table S2 show some contamination in the stock digestion solution of Ca, Br, and Pb. The differences between the stock solution and the actual sample analyses, however, were found to be at least one order of magnitude, meaning the amounts present in the samples are significantly different from those in the stock digestion solution. The samples named "Stock 1, 2, and 3" are different aliquots analyzed from the same stock solution. Each sample was run as an individual batch.

3. Optical Analysis

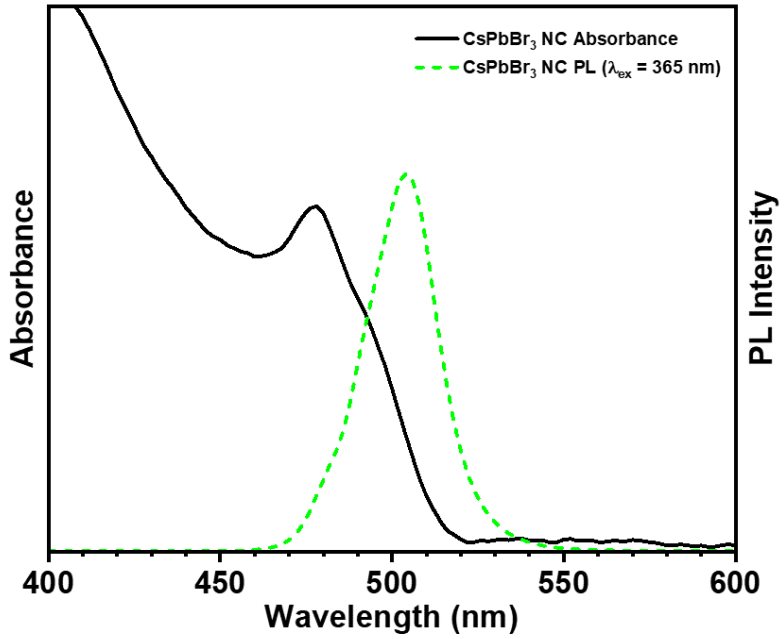

Figure S7. Absorbance and photoluminescence spectra acquired for as-synthesized $CsPbBr_3$ nanocrystals suspended in toluene.

4. Nanoparticle Analysis

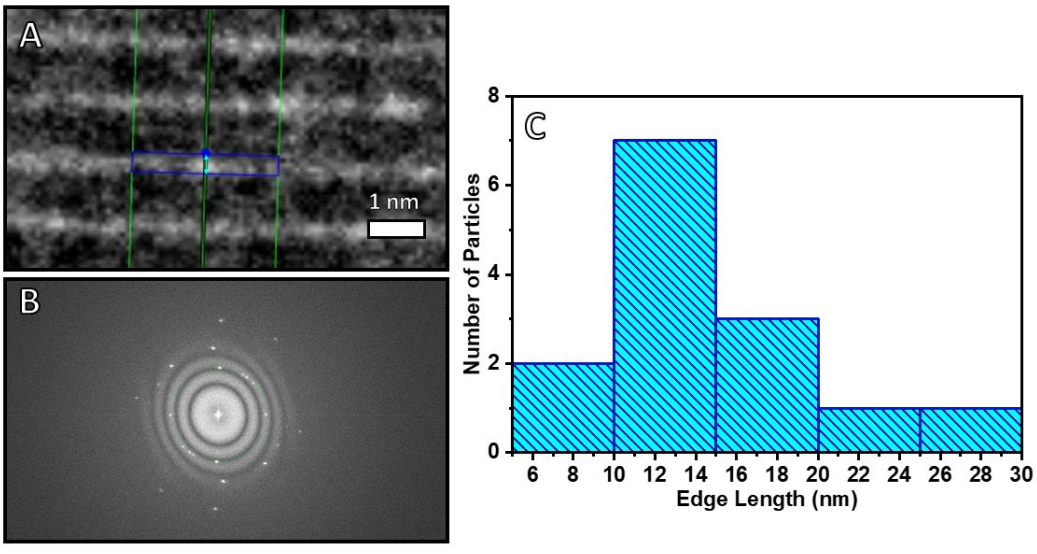

Figure S8. (A) Measurement of interplanar spacing (d-spacing) for (210) crystal plane in bright field TEM depicted by light blue arrow. (B) Fast Fourier transform (FFT) collected of observed nanoparticle. (C) Histogram of nanoparticle size.

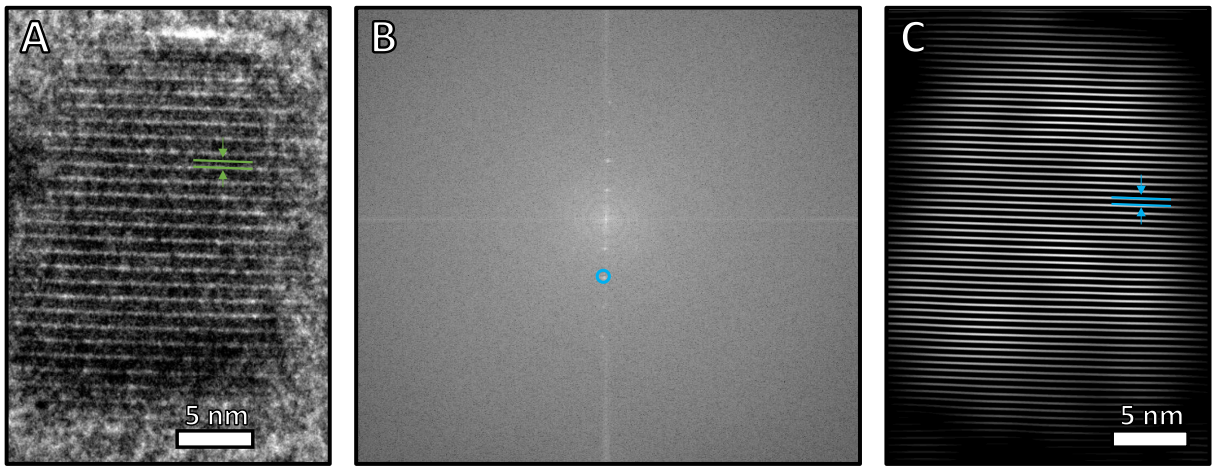

Figure S9. (A) Measurement of interplanar spacing (d-spacing) for (110) crystal plane in bright field TEM depicted by green bars. (B) Fast Fourier transform (FFT) calculated of the observed nanoparticle with the reflection (blue circle) used for (C) inverse FFT to calculate the d-spacing from lattice fringes (blue bars).